# Mineral Scales in Biological and Industrial Systems



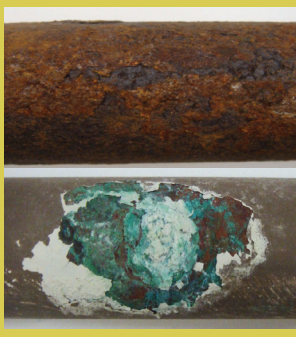
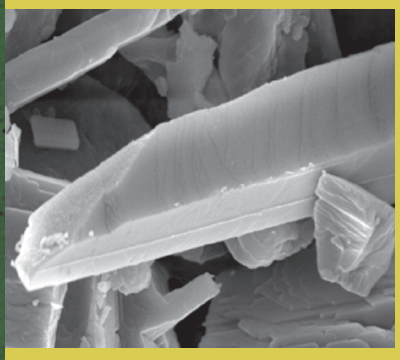
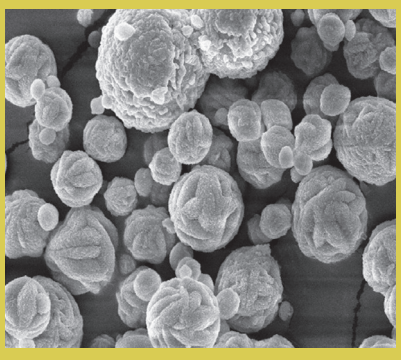
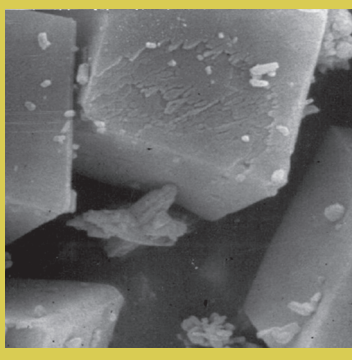

Edited by
Zahid Amjad

CRC Press
Taylor & Francis Group

# Mineral Scales in Biological and Industrial Systems

# Mineral Scales in Biological and Industrial Systems

Edited by

Zahid Amjad

CRC Press
Taylor & Francis Group
Boca Raton London New York

CRC Press is an imprint of the
Taylor & Francis Group, an **informa** business

**Cover credits:** Top left: Photograph of scaled tube. (Courtesy of Kostas Demadis.) Top center: Photo of cooling towers at a sewage treatment plant. Top upper right: Photo of brown corroded tube. (Courtesy of Zahid Amjad.) Top lower right: Photo of blue copper corroded tube. (From Amjad, Z., Controlling Copper-Based Fouling in Industrial Water Systems, *Materials Performance*, 52(3), 51 (Figure 1), © NACE International 2013.) Bottom left, center, and right: Scanning electron microscopy images of crystals.(Courtesy of Petros Koutsoukos.)

CRC Press
Taylor & Francis Group
6000 Broken Sound Parkway NW, Suite 300
Boca Raton, FL 33487-2742


Version Date: 20130919

International Standard Book Number-13: 978-1-4665-6868-6 (eBook - PDF)

# Contents

## PART IV Industrial: Suspended Matter and Oil Dispersion



## PART V Scale/Deposit Characterization Techniques

# Preface

This volume covers the proceedings of the symposium entitled "Minerals Scales in Biological and Industrial Systems," sponsored by the American Chemical Society's Division of Colloid and Surface Chemistry. The symposium was held in Philadelphia, Pennsylvania, from August 19 to August 23, 2012, as part of the 244th National Meeting of the American Chemical Society. Recognized experts in their respective fields were invited to speak at the symposium, with strong attendance particularly from academia, government, and industrial research centers.

This symposium was part of a larger series on this topic. The first symposium addressing issues related to mineral scales and deposits was held in Washington, District of Columbia, from August 21 to August 25, 1994, at the 208th National Meeting of the American Chemical Society. This symposium was organized with the following objectives in mind: (a) to bring together researchers and technologists from academia, research centers, and industries, with active interest in this topic; (b) to provide an opportunity for discussion of recent developments; (c) to offer a forum for exchange of ideas; and (d) to identify the unfulfilled needs and challenges on the control of mineral scales and deposits facing various industries.

Water available for domestic and industrial applications contains a variety of soluble and insoluble impurities such as dissolved minerals, natural organic compounds, suspended particles, and domestic and industrial wastes. If the water containing these impurities is used without any pretreatment, it leads, in many cases, to the deposition of unwanted materials on equipment surfaces (e.g., heat exchangers, pumps, pipes, and reverse osmosis membranes). The deposits commonly encountered are encompassed within six categories: (a) mineral salts; (b) corrosion products; (c) suspended matter; (d) microbiological mass; (e) oil, grease, and other debris; and (f) incompatibility of water treatment chemicals and process contaminants. Industrial water systems impacted by these unwanted deposits include boiling and cooling processes, desalination (distillation and membrane-based), geothermal power generation, milk pasteurization, oil and gas production, sugar refining, and the pulp and paper industry.

In the laundry application, insoluble mineral salts such as calcium carbonate tend to accumulate on washed fabric and washing equipment parts, resulting in undesirable fabric encrustation or scaling. In the autodishwashing application, filming and spotting of glasses and dishes by undesirable materials may be attributed to hard water and/or poor-quality detergent. The precipitation of scale-forming salts is also of primary importance in the biological system. Dental calculus, or tartar, primarily consists of salts of calcium, phosphate, and carbonate. Kidney stones generally consist of calcium oxalate and/or phosphate, and in rare cases may contain salts of uric acid, magnesium, and ammonium phosphates. In the brewery industry, calcium oxalate salts are also known to form on equipment surfaces.

A serious challenge encountered in many industrial processes is the buildup of undesirable materials on the walls of water-handling equipment, heat exchangers,

and reverse osmosis membrane surfaces. To prevent the deposition of these materials, water technologists incorporate various chemicals into the formulations, including precipitation inhibitors (polymeric and nonpolymeric), corrosion inhibitors, and dispersants. Biocides are fed separately into the system to control microbiological growth. During the last two decades, significant advances have been made in the development and application of both synthetic and environment-friendly additives for home care and industrial applications. In view of these challenges, understanding the mechanisms of scale inhibition and dispersion is of paramount importance.

This volume has 22 chapters, which can be classified into 5 parts, that mirror the structure of the symposium. Part I (Chapters 1 through 7) deals with precipitation and inhibition of various scale-forming salts, including calcium carbonate, calcium sulfate, calcium fluoride, and calcium phosphate encountered in various industrial systems such as boilers, cooling, and high-pressure and high-temperature applications. Chapters 1 and 2 are concerned with the nucleation and crystal growth of calcium carbonate in aqueous systems. In Chapter 3, discussion is presented on the application of the new environment-friendly inhibitor for high-pressure-high-temperature (HP–HT) system. Chapter 4 deals with the evaluation of biopolymers as crystal growth inhibitors for calcium sulfate dihydrate and barium sulfate scales. In Chapter 5, performance data on several inhibitors for controlling barium sulfate scale formation in HP–HT application is discussed. Chapters 6 and 7 present information on the precipitation and inhibition of calcium fluoride and calcium phosphate.

Part II is comprised of six chapters (Chapters 8 through 13), which address the precipitation and inhibition of salts commonly encountered in sugar refining (calcium oxalate, calcium phosphate) and geothermal power generation (silica and metal silicate). Chapter 8 presents discussion on the causes and the probable mechanisms of formation of calcium oxalate monohydrate and dihydrate, hydroxyapatite, calcium sulfate dihydrate and amorphous silica in sugarcane juice heat exchanger tubes. In chapter 9 results are presented on the influence of a series of potential pollutants in the recovery of phosphorus from wastewater using different crystallization techniques. The influence of various factors on precipitation and deposition of silica and metal silicate on equipment surfaces in industrial systems i.e., cooling water, desalination, geothermal, etc., is presented in Chapters 9 through 12. Additionally, these chapters also discuss the role of inhibitor architecture in preventing silica/silicate scales in industrial systems. Chapter 13 presents a "state-of-the-art" overview of antiscalant selection for desalination systems.

Part III (Chapters 14 and 15) incorporates a discussion on mineral scales that are important in biological systems. Chapter 14 describes the morphological transformation, polymorphic changes, and crystal inhibition of calcium biominerals by anionic macromolecules. Chapter 15 presents two new and important items of information on polarized hydroxyapatite (HAP) surface characteristics and cell behavior on polarized HAP.

Part IV is comprised of five chapters (Chapters 16 through 20), which deal with the control of suspended matter in industrial water systems. Chapter 16 describes the role of various physicochemical processes involved in the dispersion of suspended matter. Chapter 17 deals with the evaluation of various innovative chemicals such as oil dispersants. Chapter 18 presents performance data on the evaluation of various

biopolymers and synthetic polymers as iron oxide (rust) dispersants. Chapter 19 presents new information on the application of phosphonates as corrosion and scale inhibitors for various industrial water systems. Chapter 20 presents discussion on the role of polymer architecture in stabilizing copper (II) in aqueous systems.

Part V (Chapters 21 and 22) provides an account of the analytical techniques commonly used to characterize mineral scales and deposits formed during the in-house evaluation of new products and/or deposit samples received from industrial installations for characterization as well as product failure analyses.

This book is intended for academic researchers in the fields of biology, chemistry, dentistry, environmental and chemical engineering, geology, and medicine. It will also be useful for technology-focused researchers in the industry whose interests might be directly or indirectly related to understanding the mechanisms of scale formation and inhibition in biological and industrial systems. It is hoped that this book will stimulate interest in the development of new innovative inhibitors and dispersants and meet the unfulfilled needs of industrial and academic researchers. This book will be useful for technologists, plant managers, and process and design engineers working in industries including water treatment, petroleum refinery, industrial effluent cleaning, textile processing, and food and beverage production.

I thank everyone who contributed to this book substantively and to the symposium on which it is based. I would like to extend my gratitude to the financial contributors. A special thanks is extended to the American Chemical Society, Division of Colloid and Surface Chemistry; Avlon Industries; Chevron Corporation; Global Tungston and Powders; Lubrizol Corporation; and Unichem Technologies—without their generous assistance, the symposium would not have achieved the success it did.

I would like to express my sincere appreciation of Dr. Petros G. Koutsoukos and Dr. Michael R. Reddy for serving as chairs at the symposium. I am also grateful to Dr. Michael J. Dunphy, chairman of the Division of Mathematics and Sciences at Walsh University, for his endless encouragement and support and for permitting me to organize the symposium and to edit this book.

I am indebted to Barbara Glunn and David Fausel of CRC Press for their patience and invaluable assistance in preparing this book. Finally, I owe a special debt of gratitude to my beautiful wife, Rukhsana, and my lovely daughter, Naureen, for their constant support in the last several years. It is their constant encouragement and patience that allowed me to devote numerous evenings and weekends to this book.

**Zahid Amjad, PhD**
*Cleveland, Ohio*

# Editor

**Zahid Amjad** received his BSc in (chemistry) and MSc in (chemistry) from Punjab University, Lahore, Pakistan, and his PhD from Glasgow University, Scotland, United Kingdom. He was a lecturer at the Institute of Chemistry of Punjab University and served as an assistant research professor at the State University of New York at Buffalo, New York. He began his professional career as an R&D scientist. During his more than 30 years at Calgon Corporation, Pittsburgh, Pennsylvania, and Lubrizol Advanced Materials, Inc., Cleveland, Ohio, he has worked in various fields, including cosmetics, home care, oral care, pharmaceutics, water treatment, water purification, and related fields. His major interests include biological and industrial applications of water-soluble and water-swellable polymers, interactions of polymers with different substrates (i.e., heat exchanger, tooth enamel, membrane, hair, fabric, ceramic, pigments), crystal growth and dissolution, and adsorption and desorption phenomena in aqueous systems.

Dr. Amjad has presented invited lectures at various national and international meetings, universities, and industrial research centers. He has published over 160 technical papers, has contributed to numerous book chapters, has edited 6 books, and holds 30 US patents. He was inducted into the National Hall of Corporate Inventors and is listed in *American Men and Women of Sciences*, *Who's Who in Technology*, and *Who's Who of American Inventors*. Dr. Amjad is the recipient of the EDI Innovation Award (1997) and the recipient of the Association of Water Technologies' Ray Baum Memorial Water Technologist of the Year Award (2002). He is the owner of Aqua Science and Technology LLC, Columbus, Ohio, which provides consulting services for industrial water treatment, separation processes, and related technologies. Dr. Amjad currently serves as a visiting professor in the Division of Mathematics and Sciences at Walsh University, North Canton, Ohio.

# Contributors

**Nureddin M. Abbas**
Global Tungsten & Powders
Towanda, Pennsylvania

**Emel Akyol**
Department of Chemical Engineering
Yildiz Technical University
Istanbul, Turkey

**Zahid Amjad**
Division of Mathematics and Sciences
Walsh University
North Canton, Ohio
and
Cleveland, Ohio

**Giasemi K. Angeli**
Department of Chemistry
University of Crete
Heraklion, Greece

**Eleni C. Arvaniti**
Department of Chemical Engineering
University of Patras
and
Foundation of Research and
Technology Hellas
Institute of Chemical Engineering and
High-Temperature Chemical Processes
Patras, Greece

**Georgia D. Athanasakou**
Department of Chemical Engineering
University of Patras
and
Foundation of Research and
Technology Hellas
Institute of Chemical Engineering and
High-Temperature Chemical Processes
Patras, Greece

**Ping Chen**
Nalco Champion
Aberdeen, United Kingdom

**Tao Chen**
Nalco Champion
Aberdeen, United Kingdom

**Mitali China**
Department of Chemical and
Biological Engineering
University at Buffalo
Buffalo, New York

**Konstantinos D. Demadis**
Department of Chemistry
University of Crete
Heraklion, Greece

**Özlem Doğan**
Department of Chemical Engineering
Yildiz Technical University
Istanbul, Turkey

**William O.S. Doherty**
Centre for Tropical Crops and
Biocommodities
Queensland University of Technology
Brisbane, Queensland, Australia

**Christopher P. East**
Centre for Tropical Crops and
Biocommodities
Queensland University of Technology
Brisbane, Queensland, Australia

**Chunfang Fan**
Halliburton
Houston, Texas

**Christopher M. Fellows**
School of Science and Technology
University of New England
Armidale, New South Wales,
Australia

**Darrell L. Gallup**
Thermochem, Inc.
Santa Rosa, California

**Dominique Guyton**
Division of Mathematics
and Sciences
Walsh University
North Canton, Ohio

**Thomas Hagen**
Nalco Champion
Aberdeen, United Kingdom

**David Hasson**
Rabin Desalination Laboratory
Wolfson Department of Chemical
Engineering
Technion—Israel Institute of
Technology
Haifa, Israel

**Panayiotis I. Ioannou**
Department of Chemistry
University of Patras
Patras, Greece

**Amy T. Kan**
Brine Chemistry Consortium
Rice University
Houston, Texas

**Lisa K. Kemp**
School of Polymers and High
Performance Materials
University of Southern Mississippi
Hattiesburg, Mississippi

**Petros G. Koutsoukos**
Department of Chemical
Engineering
University of Patras
and
Foundation of Research and
Technology Hellas
Institute of Chemical Engineering and
High-Temperature Chemical Processes
Patras, Greece

**Chi Lo**
Department of Earth and
Environmental Engineering
Columbia University
New York, New York

**Robert Y. Lochhead**
School of Polymers and High
Performance Materials
University of Southern Mississippi
Hattiesburg, Mississippi

**Theano Mavrikou**
Department of Chemical
Engineering
University of Patras
Patras, Greece

**Harry Montgomerie**
Nalco Champion
Aberdeen, United Kingdom

**Danielle Morgan**
Division of Mathematics
and Sciences
Walsh University
North Canton, Ohio

**Sarah E. Morgan**
School of Polymers and High
Performance Materials
University of Southern Mississippi
Hattiesburg, Mississippi

**Ioannis Mpountas**
Department of Chemical Engineering
University of Patras
and
Foundation of Research and Technology Hellas
Institute of Chemical Engineering and High-Temperature Chemical Processes
Patras, Greece

**Miho Nakamura**
Institute of Biomaterials and Bioengineering
Tokyo Medical and Dental University
Tokyo, Japan

**Mualla Öner**
Department of Chemical Engineering
Yildiz Technical University
Istanbul, Turkey

**Christakis A. Paraskeva**
Department of Chemical Engineering
University of Patras
Patras, Greece

**Partha Patra**
Department of Earth and Environmental Engineering
Columbia University
New York, New York

**Melina Preari**
Department of Chemistry
University of Crete
Heraklion, Greece

**Michael M. Reddy**
Denver Federal Center Lakewood
U.S. Geological Survey
Lakewood, Colorado

**Stamatia Rokidi**
Department of Chemical Engineering
University of Patras
and
Foundation of Research and Technology Hellas
Institute of Chemical Engineering and High-Temperature Chemical Processes
Patras, Greece

**Daniel Savin**
School of Polymers and High Performance Materials
University of Southern Mississippi
Hattiesburg, Mississippi

**Raphael Semiat**
Rabin Desalination Laboratory
Wolfson Department of Chemical Engineering
Grand Water Research Institute
Technion—Israel Institute of Technology
Haifa, Israel

**Hilla Shemer**
Rabin Desalination Laboratory
Wolfson Department of Chemical Engineering
Technion—Israel Institute of Technology
Haifa, Israel

**Wei Shi**
Aquateam
Oslo, Norway

**Raj P. Singh Gaur**
Global Tungsten & Powders
Towanda, Pennsylvania

**P. Somasundaran**
Department of Earth and Environmental Engineering
Columbia University
New York, New York

**Mason B. Tomson**
Brine Chemistry Consortium
Rice University
Houston, Texas

**Marina Tsianou**
Department of Chemical and Biological Engineering
University at Buffalo
Buffalo, New York

**Anna Tsistraki**
Department of Chemistry
University of Crete
Heraklion, Greece

**Wei Wang**
Chevron Energy Technology Company
Houston, Texas

**Valerie P. Woodward**
Lubrizol Advanced Materials, Inc.
Cleveland, Ohio

**Kimihiro Yamashita**
Institute of Biomaterials and Bioengineering
Tokyo Medical and Dental University
Tokyo, Japan

**Yan Zong**
School of Polymers and High Performance Materials
University of Southern Mississippi
Hattiesburg, Mississippi

**Robert W. Zuhl**
Lubrizol Advanced Materials, Inc.
Cleveland, Ohio

# *Part I*

## *Industrial: Carbonate, Sulfate, Phosphate, and Fluoride Scales*

# 1 Nucleation and Crystal Growth of Calcium Carbonate under Flow Conditions

*Georgia D. Athanasakou, Eleni C. Arvaniti, Petros G. Koutsoukos, and Christakis A. Paraskeva*

## CONTENTS



## 1.1 INTRODUCTION

The deposition of sparingly soluble salts in porous formations causes severe scaling problems during oil production. The formation of scale is the cause of serious operational problems in oil and gas industry, dramatically reducing production rates. This reduction is mainly due to the formation of insoluble salts through nucleation and crystal growth within tubing, casings, and associated equipment, as well as in the well bore and the formation itself [1]. As a result, extra capital cost, substantial operating cost, and in extreme cases the abandonment of the oil wells are needed. Similar scaling problems are present in the production wells and equipment used for the utilization of geothermal energy [2], in water desalination, where scaling decreases the operational life of membranes [3], and in $CO_2$ sequestration in subsoil wells [4,5]. In oil production, the trapped oil ganglia in the pores of rock formations are displaced by forced injection of immiscible fluids, like formation water or seawater. The chemical composition of these media often favors pore plugging due to the development of locally high supersaturation with respect to calcium carbonate [6]. The most common types of scale encountered in oil fields include carbonate and sulfate salts of calcium, strontium, and barium [1,7–9].

Liu et al. [10] reported that there are several factors affecting scale formation, including temperature, partial pressure of $CO_2$, pH, and metal ion concentrations. Moreover, multiple phase flow (oil, gas, and water), tubing surface properties, flow velocity, ionic strength (IS), and the presence of ion such as $Mg^{2+}$ are also factors that should be considered in the scaling process [11].

The main motivation of the present work was the investigation on the precipitation mechanism of calcium carbonate through in situ mixing of soluble salt solutions in a flow chamber (channel) simulating the restricted conditions of pores to a first approximation. The experimental design was appropriate for the observation of the formation and subsequent development of calcium carbonate crystallites within the channel using optical microscopy. Calcium carbonate was selected in this investigation because this salt is most commonly encountered in scale deposits in porous media including oil field production wells.

### 1.1.1 Theoretical Background

Calcium carbonate ($CaCO_3$) is an interesting salt system due to its polymorphism. Therefore, many works have been reported concerning calcium carbonate precipitation [11–14]. According to Elfil and Roques [15], there are three main anhydrous crystalline polymorphs of calcium carbonate in the order of decreasing stability: the rhombohedral calcite, the prismatic aragonite, and the spherical vaterite. Three hydrate forms, amorphous calcium carbonate, monohydrate calcium carbonate, and hexahydrate calcium carbonate, have also been reported, less stable than the three anhydrous polymorphs. The precipitation of calcium carbonate polymorphs from aqueous supersaturated solutions, open to the atmosphere, may be described by the equilibria [16]:

$$CO_2(g) \leftrightarrows CO_2(aq) \tag{1.1}$$

$$CO_2(aq) + H_2O \leftrightarrows H^+(aq) + HCO_3^-(aq) \tag{1.2}$$

$$HCO_3^-(aq) \leftrightarrows H^+(aq) + CO_3^{2-}(aq) \tag{1.3}$$

$$Ca^{2+}(aq) + CO_3^{2-}(aq) \leftrightarrows CaCO_3(s) \tag{1.4}$$

The driving force for the crystal growth of calcium carbonate in aqueous supersaturated solutions is defined as the change in the values of Gibbs free energy when a supersaturated solution is driven to equilibrium:

$$\Delta G = -\frac{RT}{2} \ln SR \tag{1.5}$$

where

$R$ is the universal gas constant
$T$ (K) is the absolute temperature
$SR$ is the supersaturation ratio

The supersaturation ratio, *SR*, is given by Equation 1.6:

$$SR = \frac{a_{Ca^{2+}} \cdot a_{CO_3^{2-}}}{K^0_{s,CaCO_3}} \tag{1.6}$$

In Equation 1.6, $a$ is the activity of the subscripted ions and $K^0_{s,CaCO_3}$ is the thermodynamic solubility product of calcium carbonate polymorph considered.

Apparently, for $SR < 1$, the solution is undersaturated, and any amount of calcium carbonate present in the solution will be dissolved. For $SR > 1$, the solution is supersaturated, and the precipitation of calcium carbonate is possible, while at $SR = 1$, the solution is at equilibrium. The activities of all ions involved in the calculations of *SR* according to Equation 1.6 are related with the corresponding analytical concentrations with the activity coefficients, which in turn are a function of the ionic strength, IS, of the solutions [17]:

$$IS = \frac{1}{2} \sum_i m_i \cdot z_i^2 \tag{1.7}$$

where

$z_i$ is the charge of species $i$ in the solution
$m_i$ is the corresponding molality

In the present work, IS was kept constant at 0.15 M with the addition of NaCl as background electrolyte.

## 1.2 EXPERIMENTAL

### 1.2.1 Materials

Calcium chloride ($CaCl_2 \cdot 2H_2O$), sodium bicarbonate ($NaHCO_3$), and sodium chloride (NaCl) stock solutions were prepared from the respective crystalline, reagent-grade chemicals (Merck), using deionized, triply distilled water. The flow cells used in experiments were made from PMMA (Plexiglas®) as it was found from preliminary experiments that this material was inert from the point of view of inducing nucleation and crystal growth. The tubes for the transfer of the solutions to the cell were from Teflon®.

### 1.2.2 Experimental Setup and Scale Formation Experiments

In all experiments, the development of calcium carbonate particles was monitored through an optical microscope equipped with a digital, programmed video camera. Crystallite appearance and further evolution of crystal growth were recorded. In order to monitor the process at different distances from the injection point along the flow cells, four different semicylinder-shaped channels (diameter 1 mm and depth 30 μm) with different channel lengths (2, 6, 8, and 10 cm) as shown in Figure 1.1 were fabricated. The channel was sealed by a transparent lid from the same material,

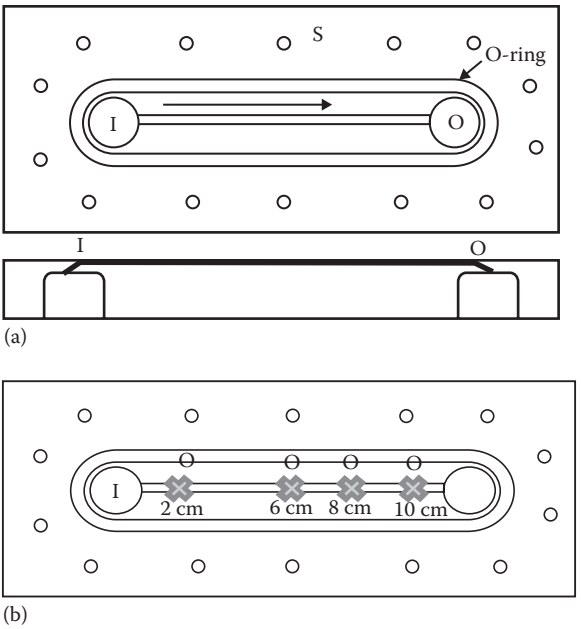


**FIGURE 1.1** (a) Schematic representation of the 2-D flow channel. Up: cross section. Down: side view. I: entry point of solution. O: outlet of solution. S: screws to tighten the lid over the flow channel. Arrow shows the direction of flow through the channel and (b) different positions of observation of crystals precipitating along the channel: 2, 4, 8, and 10 cm from the injection point of the supersaturated solutions. Each cross corresponds to the point of emergence of the effluent from the respective channel.

which was secured with screws ensuring air- and watertight sealing. This setup, besides optical monitoring, allowed for the measurement of changes of calcium concentration, precipitation rates, and supersaturation values along the flow cells in which the formation of calcium carbonate took place.

Two solutions, calcium chloride ($CaCl_2$) and sodium bicarbonate ($NaHCO_3$), were mixed just before the injection point with the aid of two syringe pumps supplying the solutions at flow rate 3.7 mm/s. Sodium chloride (NaCl) was added in both solutions to maintain IS at 0.15 M. All experiments were done at room temperature (25°C) and pressure. A microscope (Zeiss) connected with a digital camera (Axis 223M Network Camera) was used for monitoring the precipitation process. The frames were taken at specific time intervals during the course of the experiment. The advantage of using the optical microscope was the possibility to continuously record the growth of calcium carbonate crystals at different positions along the flow cell as a function of time at steady-state conditions established by the continuous flow of the supersaturated solution. The schematic layout of the experimental setup is shown in Figure 1.2.

At the outlet of each flow cell, the pH was monitored using a combined glass/Ag/AgCl electrode calibrated frequently with NBS buffer solutions, while calcium was analyzed by sampling from the outlet of the flow cell. Calcium analysis was done

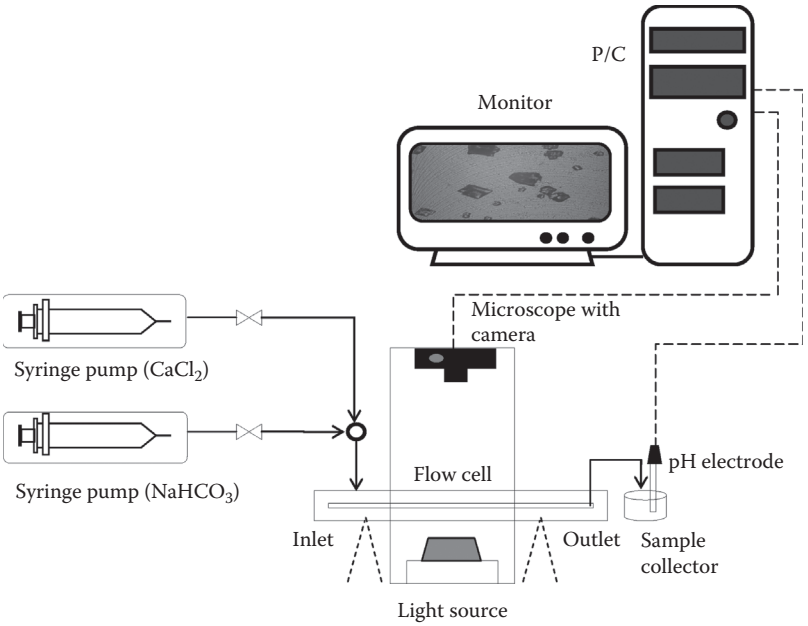


**FIGURE 1.2** Outline of the experimental setup for in situ monitoring of calcium carbonate precipitation from supersaturated solutions in flow through cells.

by atomic absorption spectrometry (Perkin Elmer Analyst 300) using air/acetylene mixture. The saturation ratio of the solutions with respect to calcite, $SR_{Calcite}$, considering the system open to the atmosphere was calculated using MULTISCALE®, a thermodynamic equilibrium modeling software [18].

## 1.3 RESULTS AND DISCUSSION

The Reynolds number, *Re*, for the system used in our experiments is normally defined in terms of a characteristic length of the flow cell. Two values of Reynolds number (flow in the channel and flow within the feed tubes) were calculated, $Re_{channel} = 1.912$ and $Re_{tube} = 0.0528$, respectively, suggesting in our experimental conditions that the flow of the supersaturated solutions was laminar. This type of flow is anticipated for the flow in porous media. Liu et al. [10] suggested that the rate of flow during water injection in the oil recovery process can affect the scaling tendency. Low water flow velocities result to higher scaling tendency. Therefore, the smaller the value of the Reynolds number, the more readily scale deposits form.

At the outlet of each of the flow cells, samples were taken and filtered through membrane filters, and the calcium concentration of the filtrates was measured using the appropriate standard solutions. Calcium concentration values measured at the outlets of flow cells decreased with time, suggesting that calcium carbonate precipitation took place inside the flow cells. The rates of precipitation in each flow cell were calculated from the change of calcium concentration over the time interval in

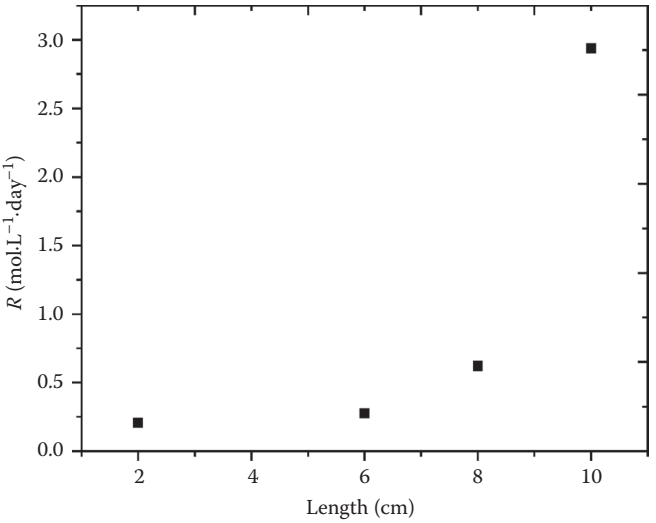


**FIGURE 1.3** Rate of precipitation of calcium carbonate (calculated from calcium concentration changes) at different distances from the entry point of the solution supersaturated with respect to calcite: 25°C, $SR = 10.7$, ionic strength 0.15 M with NaCl.

which samples were collected at the outlet of each cell, $\Delta C/\Delta t$. The rates of calcium carbonate formation, $R_p$, calculated for the four flow cells used in the present work are shown in Figure 1.3. The feed of calcium and carbonate solutions was constant thus maintaining for the growing crystals a constant supersaturation ratio environment (steady state), lower than the initial value. As expected, the values of the rates found were higher for the flow cells of longer length because of the higher residence times and the resulting larger changes in calcium concentration. In Figure 1.4, the supersaturation values at the outlet of the flow cells past 4 days, at constant initial supersaturation values ($SR_{\text{initial}} = 10.7$), are shown (temperature, flow rate, feed solution concentrations, and IS were kept constant). Supersaturation values decreased as the supersaturated solutions flowed through the flow cells, suggesting that scale formation is more intense close to the injection points. It should be noted that the *SR* at positions 3 and 4 was very close, suggesting similarity of steady-state conditions past a certain distance from the solution entry point. During the collection of the samples and the recording of pH values at the outlet of the flow cells, the formation and growth of crystals in each position were monitored as a function of time through the collection of successive frames from the camera attached to the optical microscope. A typical sequence of images captured during precipitation at each position is shown in Figure 1.5. The first visible crystal was recorded 6 h after the initiation of the experiment at position 1, while at positions 2 and 3, crystals appeared after 2 days. Only after 6 days, visible crystals were found at position 4 (10 cm from the inlet). As expected, precipitation rate and crystal growth were higher near the inlet of the channel where a large number of large crystals were observed, while only a few crystallites were found closer to the outlet of the supersaturated solutions. This observation was attributed to the fact that the supersaturation near the inlet of the

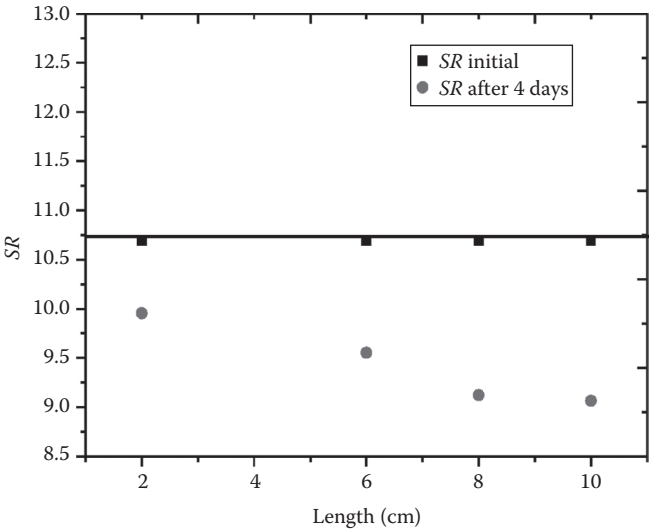


**FIGURE 1.4** The supersaturation evolution as a function of time, past 4 days from the injection of the supersaturated solution: 25°C, $SR = 10.7$, ionic strength 0.15 M with NaCl; (■) initial supersaturation for each position; (•) supersaturation at the different channel positions after 4 days of experiment.

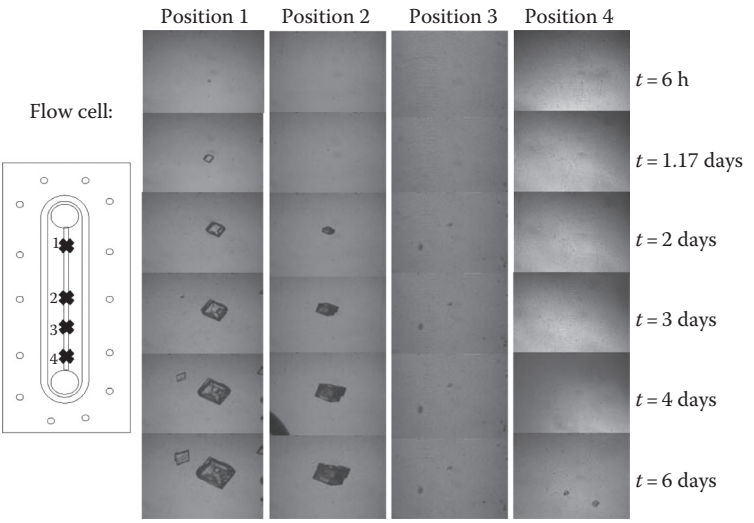


**FIGURE 1.5** Sequence of images captured during precipitation from solutions supersaturated with respect to calcite at different points of the flow cell: 2, 6, 8, and 10 cm from the entry point: 25°C, $SR = 10.7$, ionic strength 0.15 M with NaCl.

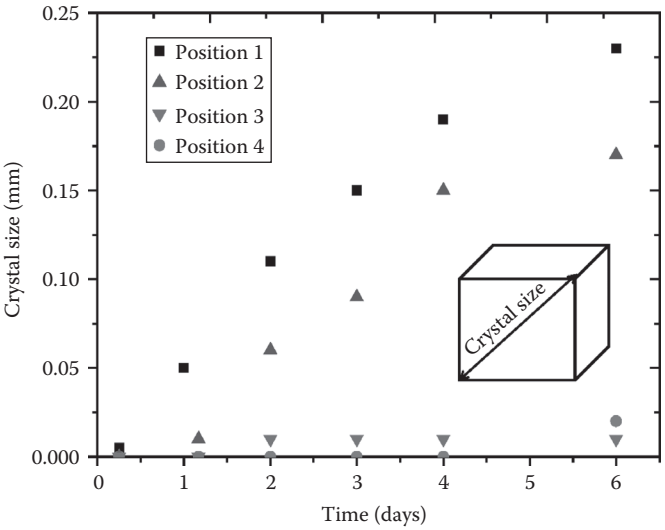


**FIGURE 1.6** Crystal size evolution during precipitation from solutions supersaturated with respect to calcite at different points of the flow cell, as a function of time. Positions 1–4: 2, 6, 8, and 10 cm from the entry point: 25°C, $SR = 10.7$, ionic strength 0.15 M with NaCl.

channel was higher resulting in higher rates of crystal growth and larger numbers of nucleated crystals that have sufficient time to grow to larger sizes. Closer to the cell outlet, the supersaturation drop was significantly larger compared to the corresponding value at the entrance, and the respective rates of crystal growth were low, resulting in smaller sizes for the initially nucleated crystallites that grew at steady-state conditions.

Examination of the pictures obtained from the first stages of crystal growth in the flow cells showed the exclusive formation of calcite crystals in all positions of observation at $SR = 10.7$. The size evolution of the crystals formed as a function of time is presented in Figure 1.6. The size of crystals was measured by an image analysis technique using Adobe Photoshop® CS5.1, with the appropriate calibration. The diagonal of the top-view of the crystals was taken as the size of the rhombohedral calcite crystals. Monitoring the evolution of crystal size, it was possible to calculate linear rates for the growth of calcite crystals in the flow cells used in the experiments. As may be seen, the linear crystal growth rate was constant up to 3 days, following which it slowed down. In positions 1 and 2, the trend was much more clearly shown, and the rates measured were significantly higher in comparison with positions 3 and 4, where the drop in solution supersaturation was much more drastic in comparison with positions 1 and 2. In positions 3 and 4, however the value of *SR* was nearly the same.

In order to investigate the effect of *SR* of the solution in the flow cells, a new series of experiments was done in which the conditions in the supersaturated solution were adjusted so that $SR_{\text{initial,calcite}} = 20$ (keeping the ratio of total calcium to total carbonate as 1). The evolution of calcium concentration measured at position 4 (exit point of the solution) for both *SR* values investigated is shown in Figure 1.7.

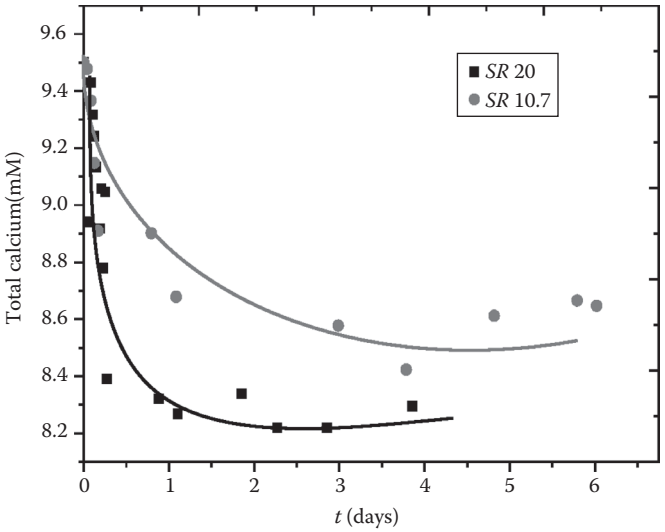


**FIGURE 1.7** Plot of the total calcium concentration as a function of time measured at position 4 (10 cm from the entry point of solutions supersaturated with respect to calcite), 25°C, ionic strength 0.15 M, $SR_i = 20$ and 10.7.

As may be seen, calcium concentration in this case was reduced at a faster rate in comparison with the corresponding measurements done for $SR_{\text{initial}} = 10.7$. The calculated rates of precipitation were consequently higher. It was thus found that the $R_p$ for $SR = 20$ was equal to 4.1 mol·L·day$^{-1}$, while at $SR = 10.7$, the corresponding value was 2.9 mol·L·day$^{-1}$. The sequence of pictures taken at position 4 (10 cm from the inlet) is shown in Figure 1.8. Indeed, for $SR = 20$, calcite crystals were identified after 6 h from the start of the experiment, while at $SR = 10.7$, only a few small crystals were recorded after 6 days. It is important also to note that in the case of $SR = 20$, the increase in crystal number was high enough to block the flow through the cell past 3 days from the start of the experiment. The trend was the same with respect to the number and size of the crystallites formed as in the case of the experiments done at $SR = 10.7$. At SR 20, therefore, it may be suggested that in the simple flow system investigated, there was an almost complete loss of permeability in 3 days' time. The number of crystal evolution as a function of time for the two values of *SR* investigated for the cell corresponding to position 4 is shown in Figure 1.9. As may be seen at high *SR* values, a large number of crystals precipitated within the flow channel. The increase in the number of crystallites shown in the sequence of photos in Figures 1.8 or 1.9 suggested that nucleation (perhaps secondary) continued in parallel with crystal growth of the nucleated crystals to larger sizes. It is also important to note that at these conditions ($SR = 20$), the formation of transient phases like vaterite and aragonite was recognized from the respective morphologies. The kinetic stabilization of transient phases has been documented in the literature for batch experiments of calcium carbonate precipitation [19]. Similar conclusions were drawn from the measurements of the linear growth rates shown in Figure 1.10.

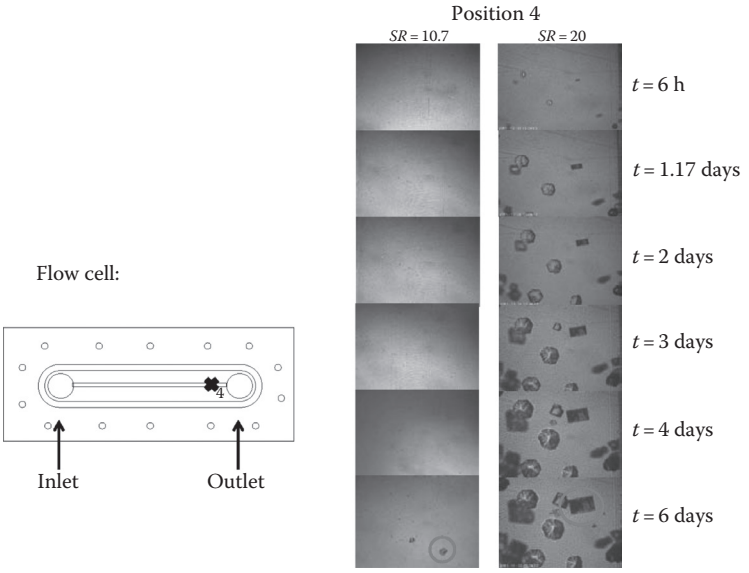


**FIGURE 1.8** Sequence of images captured during precipitation from solutions supersaturated with respect to calcite, taken at position 4 of the flow cell (10 cm from the entry point of the solutions) for $SR = 10.7$ and 20, 25°C, ionic strength 0.15 M adjusted with NaCl.

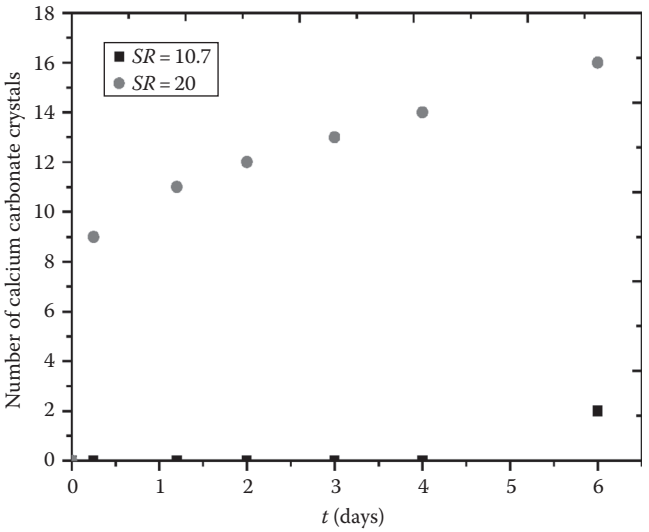


**FIGURE 1.9** Number of crystals developed in the flow channel at position 4 (10 cm from the entry point of the solution supersaturated with respect to calcite) for *SR* 10.7 and 20, 25°C, $SR = 10.7$, ionic strength 0.15 M with NaCl.

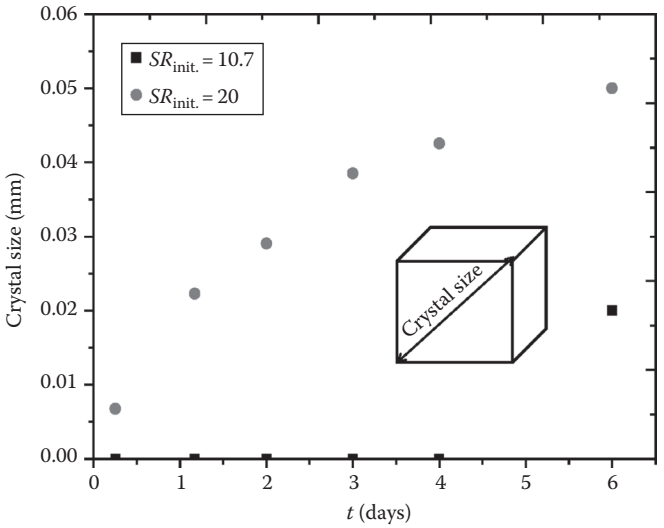


**FIGURE 1.10** Size of crystals developed in the flow channel at position 4 (10 cm from the entry point of the solution supersaturated with respect to calcite) for SR 10.7 and 20, as a function of time, 25°C, $SR = 10.7$, ionic strength 0.15 M with NaCl.

## 1.4 CONCLUSIONS

Kinetics information on the precipitation of calcium carbonate was obtained from the direct observation of the process in a transparent flow channel of 30 μm diameter constructed of PMMA, at different distances away from the entry point of solutions supersaturated with respect to calcite at two different supersaturations ($SR = 10.7$ and 20). The measurement of the number and sizes of the crystals was done through a microscope placed above the flow cell, while at the exit point of the solution from the cell, parameters including pH and calcium concentrations were continuously monitored. These measurements allowed for the calculation of crystal growth rates at four different distances from the entry point of the solution: 2, 6, 8, and 10 cm. At both *SR* values investigated, the number and size of crystals decreased along the distance from the entry point of the supersaturated solutions in the flow cell concomitant with the reduction of the *SR*. At lower supersaturation, only calcite crystals formed, while at higher supersaturations, transient phases were also identified. At low *SR* values, only few crystals were nucleated that continued to grow, while at higher values of *SR*, secondary nucleation was found through which more crystals were developed for longer time periods. An important conclusion concerning scale formation in channels, which may be considered as a 2-D pore model, is that the deposition of scale along the path of flow of the supersaturated solutions is not uniform, and the disproportionate development of scale near the entry point of supersaturated solutions may lead to full loss of permeability.

## REFERENCES


1. Merdhah, A. B. and Yassin, A. A. Scale formation in oil reservoir during water injection at high-salinity formation water. *Journal of Applied Sciences*, 7, 3198–3207 (2007).
2. Garcia, V. A., Thomsen, K., and Stenby, E. H. Prediction of mineral scale formation in geothermal and oilfield operations using the extended UNIQUAC model, Part II. Carbonate-scaling minerals. *Geothermics* 35, 239–284 (2006).
3. Antony, A., Low, J. H., Gray, S., Childress, A. E., Le-Clech, P., and Leslie, G. Scale formation and control in high pressure membrane water treatment systems: A review. *J Membr Sci* 383, 1–16 (2011).
4. Shukla, R., Ranjith, P., Haque, A., and Choi, X. A review of studies on $CO_2$ sequestration and caprock integrity. *J Fuel* 89, 2651–2664 (2010).
5. Bachu, S. Sequestration of $CO_2$ in geological media in response to climate change: Road maps for site selection using the transform of the geological space into the $CO_2$ phase space. *J Energ Convers Manag*, 43, 87–102 (2002).
6. El-Said, M., Ramzi, M., and Abdel-Moghny, T. Analysis of oilfield waters by ion chromatography to determine the composition of scale deposition. *Desalination* 249, 748–756 (2009).
7. Moghadasi, J., Muller-Steinhagen, H., Jamialahmadi, M., and Sharif, A. Model study on the kinetics of oil field formation damage due to salt precipitation from injection. *J Pet Sci Eng* 43, 201–217 (2004).
8. Atkinson, G. and Mecik, M. The chemistry of scale prediction. *J Petr Sci Eng* 17, 113–121 (1997).
9. Oddo, J. and Tomson, M. B. Why scales form and how to predict it. *Soc Petr Eng* 47–54 (1994).
10. Liu, X., Jungang, L., Qianya, Z., Jinlai, F., Yingli, L., and Jingxin, S. The analysis and prediction of scale accumulation for water-injection pipelines in the Daqing Oilfield. *J Pert Sci Eng* 66, 161–164 (2009).
11. Nancollas, G. H. and Reddy, M. M. The crystallization of calcium carbonate II. Calcite growth mechanism. *J Colloid Interface Sci* 37, 824–830 (1971).
12. Sohnel, O. and Mullin, J. W. Precipitation of calcium carbonate. *J Crystal Growth* 60, 239–250 (1982).
13. Xyla, A. G., Giannimaras, E. K. and Koutsoukos, P. G. The precipitation of calcium carbonate in aqueous solutions. *Colloids Surf* 53, 241–255 (1991).
14. Sabbides, T. G. and Koutsoukos, P. G. The crystallization of calcium carbonate in artificial seawater, role of the substrate. *J Crystal Growth* 133, 13–22 (1993).
15. Elfil, H. and Roques H. Role of hydrate phases of calcium carbonate on the scaling phenomenon. *Desalination* 137, 177–186 (2001).
16. Flaten, E. M., Seiersten, M., and Andreassen, J. P. Induction time studies of calcium carbonate in ethylene glycol and water. *J Chem Eng Res Design* 88, 1659–1668 (2010).
17. Atkins, P. *Physical Chemistry,* 8th edn., Oxford University Press, Oxford, U.K. (2006).
18. Kaasa, B. Prediciton of pH, mineral precipitations and multiphase equilibria during oil recovery, Dr. Ing. thesis, Norwegian University of Technology and Science NTNU, Trondheim, Norway (1998).
19. Spanos, N. and Koutsoukos, P. G. Kinetics of precipitation of calcium carbonate in alkaline pH at constant supersaturation. Spontaneous and seeded growth. *J Phys Chem* 102, 6679–6684 (1998).

# 2 Calcite Growth Rate Inhibition by Low Molecular Weight Polycarboxylate Ions

*Michael M. Reddy*

## CONTENTS



## 2.1 INTRODUCTION

The calcium carbonate mineral scale formation occurs in industrial and biological systems including commercial water treatment [1,2], desalination [3–6], and biocalcification [7,8]. Carbonate minerals form resistant scales (due to water hardness)

that reduce industrial process efficiency. Scale formation on heat exchanger surfaces and reverse osmosis membranes, for example, is a common operational problem in desalination technology [3,4].

Carbonate mineral scales encountered in industrial processes are often reduced or eliminated by the use of calcium carbonate crystal growth inhibitors [5,9,10], known as "threshold inhibitors," which reduce or eliminate scale by inhibiting calcium carbonate formation rates at low solution concentrations [1,2,6]. Common calcium carbonate scale formation inhibitors include polyphosphates, phosphonates [1], and poly (acrylic acid) [11,12]. Simple organic and inorganic ions including, phosphate [13], glycerophosphate [13], inositol phosphate [2], and magnesium ion [14,15], are also calcium carbonate crystal growth rate inhibitors.

Scale control threshold inhibitors added to industrial process water often contribute to water quality concerns in lakes and rivers by increasing nutrient loading and subsequent eutrophication potential [6]. However, threshold inhibitors without limiting nutrients (i.e., phosphorus [P]), such as carboxylic acid oligomers and polymers, have a range of activity as calcite growth rate inhibitors [11,12,16–18]. Natural polycarboxylic acids (PCAs) (i.e., fulvic acids [FAs]) have low phosphorus contents, are effective crystal growth inhibitors, and may have commercial applications as threshold inhibitors. FA growth inhibition properties vary with molecular weight, functional group character, and functional group ionization [19].

Geochemical research has demonstrated that surface and groundwaters form calcium carbonate scale in a range of natural environments (e.g., in rock [20], caves, streams, and lakes [21–23]) by physical and chemical processes including temperature increases, carbon dioxide outgassing, photosynthetic utilization of carbon dioxide, and so on. Natural organic matter crystal growth inhibitors, often at high concentrations (see, e.g., [23,24]), modify these processes. In Pyramid Lake, NV, for example, persistent calcium carbonate supersaturation is attributed to the presence of natural organic crystal growth rate inhibitors (e.g., FAs) as well as phosphate ion and magnesium ion [23].

Carbonate mineral formation in soils and in soil solution has important biogeochemical consequences for the global carbon cycle and sequestration of anthropogenic carbon dioxide emissions [25–27]. For example, carbonate mineral heterogeneous reactions mediate carbon dioxide transfer between soils and the atmosphere [28]. Desert soil pedogenic calcite, an important indicator of paleoclimate and landscape age, forms as a result of inorganic calcium carbonate mineralization and biomineralization by soil microorganisms [29,30]. Calcium carbonate formation rates in soils may be reduced by natural crystal growth rate inhibitors such as FA [19,31], magnesium ion [14,32], and phosphorus-containing anions (e.g., phosphate [2] and inositol hexakisphosphate [33]).

Typically, effective calcite growth rate inhibitor concentrations are much lower than that of calcium ion in solution, and the percent of calcium ion complexed in a solution containing one mg/L inhibitor concentration, for example, is less than 5%. In contrast, most inhibitor molecules exist in solution as neutral or charged calcium complexes [34], which inhibit calcite crystallization rates by surface adsorption rather than by simple calcium–inhibitor complex formation [13,14]. A Langmuir-type adsorption model often describes calcium carbonate crystal growth by simple ionic inhibitors [13,14]. Polyanion inhibitor (e.g., such as polyacrylic acid [PAc])

effectiveness is associated with inhibitor ionic charge, number of ionizable groups, functional groups, and molecular weight [19,34].

Calcite coatings on rocks and soil, similar to mineral scales observed in commercial and biological applications, are often found in arid region soils and in alkaline lake sediments [31,35]. Natural PCA inhibitors, such as FAs, occurring in municipal and industrial water supplies, and industrial cooling waters [24,36–38], modify calcium carbonate mineral formation processes, leading to persistent calcite supersaturation in some alkaline surface waters [24,35,38]. Occurrence of calcium carbonate coatings and deposits in a wide range of geological environments prompted the examination of calcite growth rate inhibition by natural polycarboxylate ions and identification of calcite growth rate inhibition functional groups present in natural polycarboxylate ions.

Naturally occurring PCAs, exhibiting significant calcite growth rate inhibition [2,11,19], have been identified using fractionation procedures, detailed chemical analysis, structural modeling, and model compound studies [24,36,37]. Moreover, calcite growth rate mediation by natural FAs may impact biocalcification rates in acidified ocean water enhancing the impact of anthropogenic $CO_2$ emissions on ocean calcification processes [7].

Despite the importance of calcium carbonate formation in industrial processes and in biological systems, and the impact of calcium carbonate formation and dissolution on the global carbon cycle, the influence of PCA constituents of FA on calcium carbonate heterogeneous reaction rates, their mechanism of interaction with calcite crystal growth sites, and their use as threshold mineral crystal growth rate inhibitors have not been well studied.

The constant composition technique, selected to characterize the influence of PCAs on calcite crystal growth rates, provides calcite growth kinetic information at fixed supersaturation levels within the calcium carbonate metastability zone at 25°C [31,39]. Experimental solutions have uniform composition through the thermostated reaction cell, and calcite crystal growth rate measurements are stable and reproducible. These reliable and reproducible experimental conditions allow the determination of calcite growth rates under known and well-controlled conditions. PCA influence on calcite crystal growth rate inhibition was determined by employing varying concentrations of alicyclic and acyclic PCAs in calcite crystal growth rate experiments. Calcite growth rates are determined in the absence and presence of structurally related FA component PCAs (two acyclic and seven alicyclic PCAs), with structural characteristics similar to structural components of FAs [19,31,36,37]. Understanding PCA structure–function relations with respect to calcite crystal growth rates, with a focus on acyclic and alicyclic PCAs of related structure and similar to subunits of FA, is an important goal of this work.

## 2.2 EXPERIMENTAL

### 2.2.1 Materials and Methods

Analytical reagent grade chemicals (except where noted) and distilled water are used in all experiments. Tetrahydrofuran-2r,3t,4t,5c-tetracarboxylic acid (THFTCA), 1,2,3,4-cyclopentane tetracarboxylic acid (CPETCA), 1,2,3,4,5,6-cyclohexane

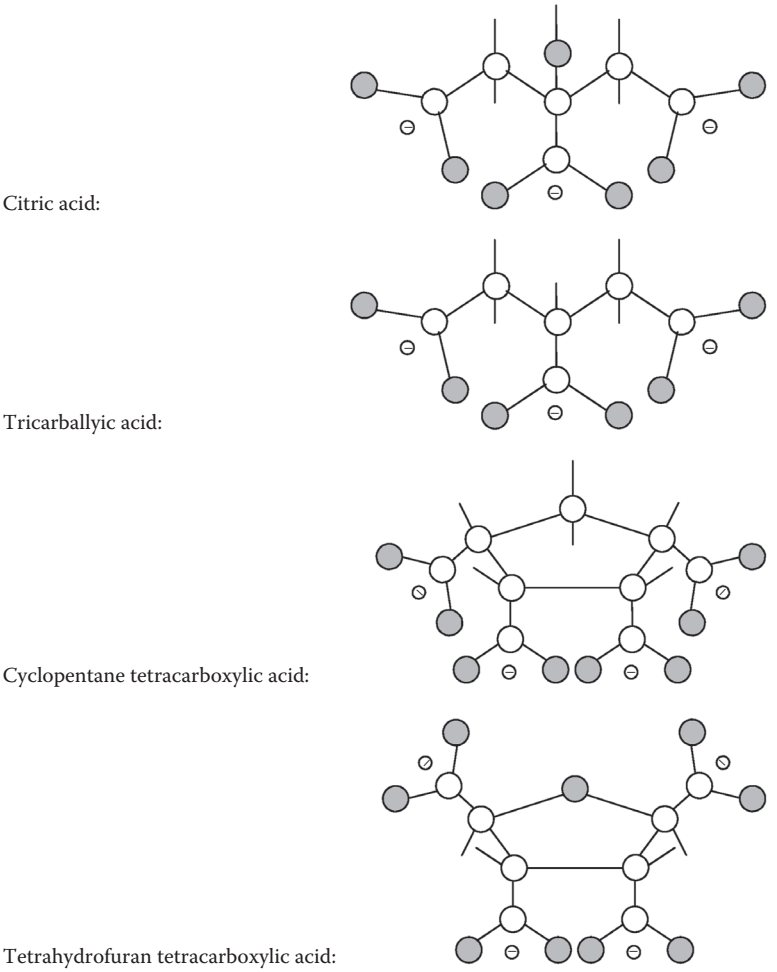


**FIGURE 2.1** Schematic diagram of four model compounds used in this study. Shaded circles represent oxygen atoms and open circles represent carbon atoms.

hexacarboxylic acid (CHXHCA), 1,1-cyclopropane dicarboxylic acid (CPRDCA), 1,1-cyclopentane dicarboxylic acid (CPEDCA), and 1,1-cyclobutane dicarboxylic acid (CBDCA) purchased from TCI America, 9211 North Harborgate Street, Portland, OR, 97303 (Figure 2.1) (the use of trade names is for identification purposes only and does not constitute endorsement by the US Geological Survey) were used as received. Table 2.1 and published analyses [40] illustrate that PCAs used contain at most trace levels of impurities that may modify the calcite growth rate inhibition properties of the model compounds. Citric acid monohydrate (CA) (purchased from the J. T. Baker Chemical Co, Phillipsburg, NJ) and tricarballylic acid (TC) (purchased from the Aldrich Chemical Co, Milwaukee, WI) were used without further purification.

**TABLE 2.1**
**Elemental Analysis of Three Model Compounds**

| | Cyclopropane Dicarboxylic Acid | | Cyclopentane Tetracarboxylic Acid | | Tetrahydrofuran Tetracarboxylic Acid | |
|---|---|---|---|---|---|---|
| Abbreviation | CPRDCA | | CPETCA | | THFTCA | |
| Chemical formula | $C_3H_4(COOH)_2$ | | $C_5H_6(COOH)_4$ | | $C_4H_4O(COOH)_4$ | |
| Gram formula weight | | 130.1 | | 246.17 | | 248.15 |
| | Measured | Theoretical | Measured | Theoretical | Measured | Theoretical |
| Loss on drying % | 7.69 | | 0.11 | | 0.49 | |
| Carbon % | 46.67 | 46.16% | 43.97 | 43.91% | 38.85 | 38.72% |
| Hydrogen % | 4.73 | 4.66% | 4.07 | 4.10% | 3.24 | 3.26% |
| Oxygen % | 47.91 | 49.19% | 51.82 | 52.00% | 56.45 | 58.03% |
| Nitrogen % | <.01 | 0.00% | <.01 | 0.00% | 0.02 | 0.00% |
| Ash % | 0.10 | | 0.01 | | <.05 | |
| Sum (after drying) | 99.41 | 100.01% | 99.87 | 100.01% | 98.56 | 100.00% |

Compounds selected for calcium carbonate growth rate inhibition properties were representative subunits of proposed FA structures [24,36–38]. In particular, compounds selected for the study included multiple carboxylate groups attached to two simple acyclic molecules and multiple carboxylate groups attached to small 3-, 4-, 5-, and 6-member ring structures. In general, pure compound inhibitors are more effective than natural PCA inhibitors because only a portion of the natural PCAs are active in calcite growth rate inhibition. Many PCAs have no effect as calcite growth rate inhibitors.

Stereochemical configurations of THFTCA and CPETCA were identified by comparing the infrared spectra of cyclic anhydrides of these compounds with standards of known stereochemical configuration. The cyclic anhydrides were synthesized by dissolving these compounds in acetic anhydride followed by evaporation to dryness. Infrared spectra were obtained employing potassium bromide pellets on a Perkin Elmer System 2000 FT-IR. The THFTCA was in the 2r,3t,4t,5c-configuration, and the CPETCA was in the *cis*, *cis*, *cis*, *cis*-configuration (Figure 2.1).

Experimental details and solution preparation are described in detail elsewhere [19,31,40]. Briefly, solutions prepared using doubly distilled water and American Chemical Society reagent-grade chemical were filtered through a 0.1 μm Whatman filter before use. Grade A glassware was used for all experiments. Growth experiments were done in a double walled Pyrex® glass cell (with a Teflon® sealed cap) placed on a stir plate and connected to a constant-temperature bath that maintained the reaction cell at a temperature of 25°C ± 0.1°C (Figure 2.2). Supersaturated solutions were magnetically stirred by a Teflon® coated stirring bar to ensure homogeneous reactor solution composition, and full and uniform suspension of the added calcite seed material.

### 2.2.2 Solution Analysis

Solution calcium concentrations, before and after growth rate measurement experiments, are measured with the ethylenediaminetetraacetic acid (EDTA)–calcein

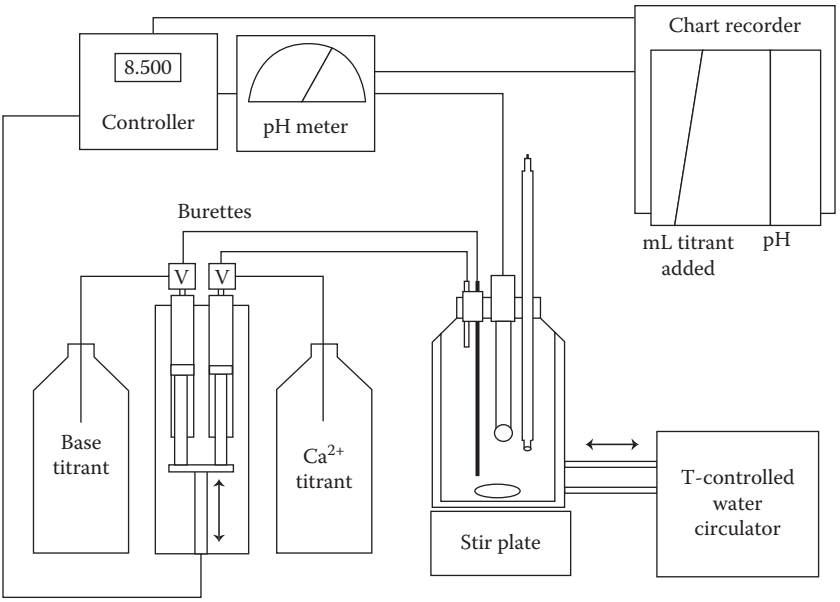


**FIGURE 2.2** Diagram of the constant composition experimental system.

complexometric method [41]. Alkalinity, before and after calcite-seeded growth experiments, is determined using a Radiometer model ABU 91 automatic titrator. Sample pH and volume of titrant added are recorded each second during calcite growth rate measurements.

### 2.2.3 Calcite Growth Rate Measurements

Solution $\Omega_c$ values describe calcium carbonate mineral formation tendency and are defined as

$$\Omega_c = \frac{[Ca^{+2}][CO_3^{-2}]}{K_{sp}}, \tag{2.1}$$

where

brackets refer to calcium and carbonate ion activities in solution
$K_{sp}$ is the calcite thermodynamic solubility product at 25°C
Solution speciation and $\Omega_c$ are calculated with the WATEQ4F program of Ball and Nordstrom [42]

Growth rate measurement solutions contain total calcium concentration of 0.0019 M, total carbonate concentration of 0.0019 M, pH ~ 8.5, ionic strength of 0.1 M maintained with potassium nitrate background electrolyte, carbon dioxide partial pressure of $10^{-3.55}$ atm, and $\Omega_c$ of 4.5 (Table 2.2). Aragonite supersaturation is 3.2, vaterite supersaturation is 1.2, and other calcium carbonate hydrated

**TABLE 2.2**
**Experimental Conditions for All Experiments**

| T (°C) | pH | $\Omega_c$ | I (M) | $[Ca]_{TOTAL}$ (M) | $[CO_3]_{TOTAL}$(M) | $P_{CO_2}$ (atm) |
|---|---|---|---|---|---|---|
| 25 ± 0.1 | 8.52 ± 0.01 | 4.5 | 0.1 | 0.0019 | 0.0019 | $10^{-3.55}$ |

phases and an amorphous phase are subsaturated in the calcite seeded growth solution. Reproducibility of the crystal growth rates among different experiments is satisfactory [19]. Mean calcite growth rate for two control experiments was $7.055 \pm 0.495 * 10^{-5}$ (±6.6%) in units of moles of calcium carbonate formed per (square meter of seed surface area [SA] per minute) (mol/[$m^2$*min]) (Table 2.3).

### 2.2.4 Experimental Conditions

Atmospheric carbon dioxide exchange with reactor solutions was minimized by keeping all reactor openings sealed during experiments. Working volume of the experimental solution is sufficient to minimize the dead volume above the supersaturated solution. Isolation from atmospheric carbon dioxide was verified by demonstrating a stable supersaturated solution pH over a 24 h test period. Seed addition was done rapidly—solution carbon dioxide exchange with atmospheric carbon dioxide during opening the reaction vessel was minimal and was very slow compared to the time needed to add seed material.

### 2.2.5 Constant Composition Experiment

Constant solution chemical composition during each experiment maintained constant calcite supersaturation by potentiometrically controlled addition of lattice ions (as calcium ion and carbonate ion), enabling accurate determination of growth rates in the absence and presence of added substances (Figure 2.2).

The calcite growth reaction at pH ~ 8.5 can be written as

$$Ca^{2+} + HCO_3^- = CaCO_{3\,solid} + H^+. \tag{2.2}$$

During calcite seeded crystallization, decreasing pH causes the double burette (Figure 2.2) system to add calcium chloride and sodium carbonate titrant solutions (at 5x reactor solution concentration). Titrant solutions contained potassium nitrate to maintain constant ionic strength. Measurement of total dissolved calcium ion concentration and alkalinity before and after all experiments verified constant reactor solution composition. Experiments were typically 100 min in duration.

### 2.2.6 Seeded Growth Conditions

Metastable working solutions, prepared prior to the start of each experiment by drop-wise addition of calcium solutions to carbonate solution in the reaction cell, are stable for at least 24 h. Ionic strength was maintained at 0.1 M. Seed material

**TABLE 2.3**
**Summary of Results for Experiments in the Absence and Presence of Alicyclic and Acyclic Polycarboxylic Acids**

**Alicyclic Polycarboxylic Acids**

| Compound | Inhibitor Concentration (mg/L) | Rate mol/ ($m^2$*min) | $r^2$ |
|---|---|---|---|
| Control | 0.00 | $6.56 \times 10^{-5}$ | 0.9979 |
| Control | 0.00 | $7.55 \times 10^{-5}$ | 0.9984 |
| CPETCA[a] | 1.00 | 0 | NA |
| CPETCA | 1.00 | $7.61 \times 10^{-9}$ | 0.004 |
| CPETCA | 0.10 | $1.90 \times 10^{-8}$ | 0.0155 |
| CPETCA | 0.10 | $01.71 \times 10^{-8}$ | NA |
| CPETCA | 0.01 | $1.67 \times 10^{-5}$ | 0.9967 |
| CPETCA | 0.01 | $1.31 \times 10^{-5}$ | 0.9879 |
| THFTCA[b] | 1.00 | $1.33 \times 10^{-8}$ | 0.0019 |
| THFTCA | 1.00 | $7.61 \times 10^{-8}$ | 0.0426 |
| THFTCA | 0.10 | $2.91 \times 10^{-5}$ | 0.9983 |
| THFTCA | 0.10 | $2.45 \times 10^{-5}$ | 0.9977 |
| *Acyclic polycarboxylic acids* | | | |
| Control | 0.00 | $9.97 \times 10^{-5}$ | 0.9990 |
| Control | 0.00 | $9.78 \times 10^{-5}$ | 0.9993 |
| Tricarballylic acid | 1.00 | $1.07 \times 10^{-4}$ | 0.9993 |
| Tricarballylic acid | 1.00 | $1.12 \times 10^{-4}$ | 0.9990 |
| Tricarballylic acid | 10.00 | $7.76 \times 10^{-5}$ | 0.9985 |
| Tricarballylic acid | 10.00 | $1.04 \times 10^{-4}$ | 0.9989 |
| Citric acid | 1.00 | $7.57 \times 10^{-5}$ | 0.9986 |
| Citric acid | 1.00 | $6.70 \times 10^{-5}$ | 0.9991 |
| Citric acid | 10.00 | $6.58 \times 10^{-5}$ | 0.9979 |
| Citric acid | 10.00 | $6.35 \times 10^{-5}$ | 0.9992 |

NA = not applicable.

Experimental conditions: T = 25°C; pH = 8.52 ± 0.02; $\Omega_c$ (calcium carbonate ion activity product/$K_{sp}$) = 4.5; $[Ca]_{TOTAL} = [CO_3^{-2}]_{TOTAL} = 0.0019$ M; $PCO_2 = 10^{-3.55}$ atm.

[a] CPETCA = 1,2,3,4-cyclopentane tetracarboxylic acid (five-carbon ring).

[b] THFTCA = tetrahydrofuran-2r,3t,4t,5c-tetracarboxylic acid (four carbon and an oxygen ring).

(Baker Analyzed Reagent calcium carbonate, J. T. Baker Chemical Company, Lot number 26832) used was analyzed by x-ray diffractometry and was free of any mineral phases other than calcite. Specific surface area (0.256 ± 0.008 $m^2/g$ (±3%)) was estimated by a three-point nitrogen adsorption technique [43]. Organic acid solutions (filtered through 0.1 μm Whatman™ cellulose nitrate filters and used within 36 h) were prepared in sodium carbonate working solutions.

### 2.2.7 Calcite Growth Rate Determination

Calcite crystal growth experiments were carried out with varying inhibitor concentrations. TC, CA, CPEDCA, CPRDCA, and CBDCA were used in experiments at concentrations up to 10 mg/L. Experiments were initiated by rapid addition of dry seed material to the solutions. A computer and chart recorder monitored titrant addition in response to calcite growth. Slope of the line representing the added titrant versus time is a direct measure of calcite growth and is converted to crystal growth rates by the following equation:

$$\text{Rate (mol/(m}^2*\text{min))} = \text{slope}$$

$$(\text{L/min})*m_{\text{titrant}}(\text{mol/L})/(\text{mass}_{\text{seed}}(\text{g})*\text{SA}_{\text{seed}}(\text{m}^2/\text{g}) \quad (2.3)$$

Experiments yielded linear plots for titrant addition over time ($r^2 > 0.995$ for control experiments); and experiments with effective calcite growth rate inhibitors gave linear plots with lower r-squared values.

Experiments using CPEDCA began as control measurements without added CPEDCA. After 100 min of growth in the absence of added CPEDCA, a stock solution of CPETCA (0.215 mL for the 1 mg/L measurement) was added to the seeded supersaturated solution to bring the solution concentration to 1, 5, 10, and 20 mg/L, respectively, over the duration of the experiment. A calcite growth rate was obtained at each CPEDCA concentration level before the addition of stock CPEDCA solution.

### 2.2.8 Calcite Growth Rate in the Presence of PCAs

Relative growth rate inhibition by PCAs in comparison to calcite growth rates in solutions without added organic material is expressed as reduced rates $R/R_0$ for each experiment:

$$\frac{R}{R_0} = \frac{\text{Rate in the presence of inhibitor}}{\text{Rate in the absence of inhibitor}} \quad (2.4)$$

Thus, a smaller reduced rate indicates greater growth inhibition.

Upon completion of experiments, solutions were rapidly filtered through 0.45 μm Whatman™ cellulose nitrate membrane filters. The filters with the crystals were air dried for 15 min at 50°C. Selected crystal samples were viewed in secondary electron mode on a JEOL scanning electron microscope (SEM) at the Denver Federal Center in Lakewood, CO.

## 2.3 RESULTS AND DISCUSSION

### 2.3.1 Calcite Growth Rates in the Absence and Presence of Several PCAs

Supersaturated solutions are stable for at least 24 h. PCAs did not initiate calcium carbonate nucleation or growth in the reaction vessel in the absence of added seed crystals. Calcite growth begins immediately upon the addition of seed, and plots of added reagent versus time are linear over the duration of the experiment except for

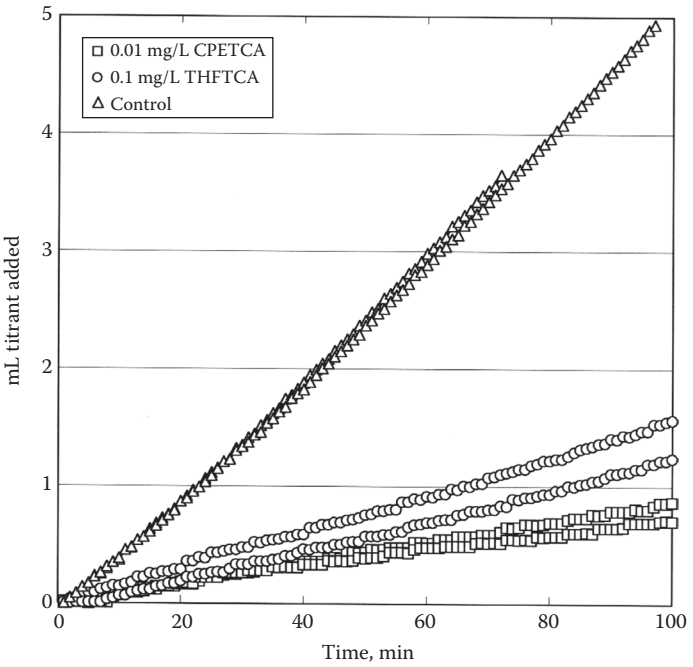


**FIGURE 2.3** Calcite crystal growth-rate measurements expressed as plots of milliliters of titrant added versus time (in minutes) for calcite seeded growth in the presence and absence of PCAs at constant supersaturation. During each experiment, the calcite growth amount varies linearly as a function of time. Calcite crystal growth rates are calculated from the slopes of the best-fit lines for plots of milliliters of titrant added versus time (in minutes). The legend indicates the CPETCA and THFTCA concentrations in mg/L.

experiments with CPETCA at concentrations of 0.01 mg/L (Figure 2.3). Replicate control experiments and experiments in the presence of several alicyclic or acyclic PCAs demonstrate good reproducibility (Figure 2.3 and Tables 2.3 and 2.4). Calcite is the only calcium carbonate phase observed in the seeded growth experiments.

Small changes occur in the measured control rates over time [24]. In order to understand these small changes, seed crystal "baking experiments" were conducted to remove seed crystal organic material prior to the start of the growth experiment. The baking process lowered, but did not eliminate, organic material on the seed crystal surface. The difference in the calcite growth rate between the unbaked seed crystals and the baked seed crystals in the absence of inhibitors is not significant at the 95% confidence level [24]. Similar experiments were also done in the presence of inhibitor ions in the growth solution [19,24]. Results of these experiments also demonstrate that organic matter adsorbed onto calcite surfaces prior to addition to the supersaturated solution has no significant influence on the measured calcite seeded growth rates in pure solutions and in solutions containing a calcite growth rate inhibitor. These experiments also demonstrate the reliability and reproducibility of the control and inhibitor-containing measured calcite seeded crystal growth rates.

**TABLE 2.4**
**Summary of Results for Experiments in the Absence and Presence of Three-Carbon, Four-Carbon, and Six-Carbon Alicyclic Polycarboxylic Acids**

| Compound | Inhibitor Concentration (mg/L) | Rate mol/ ($m^2$*min) | $r^2$ |
|---|---|---|---|
| Control-35 | 0 | $1.10\times10^{-4}$ | 0.9986 |
| CHXHCA[a] | 1 | 0 | NA |
| CHXHCA | 1 | 0 | NA |
| CHXHCA | 0.1 | $1.52\times10^{-6}$ | 0.4463 |
| CHXHCA | 0.1 | $1.14\times10^{-6}$ | 0.2682 |
| CHXHCA | 0.01 | $4.72\times10^{-5}$ | 0.9651 |
| CHXHCA | 0.01 | $2.70\times10^{-5}$ | 0.9676 |
| CHXHCA | 0.03 | $3.04\times10^{-6}$ | 0.6431 |
| CHXHCA | 0.03 | $2.47\times10^{-6}$ | 0.5272 |
| CPRDCA[b] | 1 | $1.04\times10^{-4}$ | 0.9986 |
| CPRDCA | 1 | $1.18\times10^{-4}$ | 0.9974 |
| CPRDCA | 5 | $1.21\times10^{-4}$ | 0.9989 |
| CPRDCA | 5 | $1.22\times10^{-4}$ | 0.9989 |
| CPRDCA | 10 | $1.18\times10^{-4}$ | 0.9982 |
| CPRDCA | 10 | $1.23\times10^{-4}$ | 0.9992 |
| CBDCA[c] | 1 | $1.25\times10^{-4}$ | 0.9987 |
| CBDCA | 1 | $1.18\times10^{-4}$ | 0.9988 |
| CBDCA | 10 | $1.01\times10^{-4}$ | 0.9983 |
| CBDCA | 10 | $1.15\times10^{-4}$ | 0.9987 |

CPEDCA experiments did not exhibit a change in the control slope during step additions of inhibitor.

NA = not applicable.

Experimental conditions: T = 25°C; pH = 8.52 ± 0.02; $\Omega_c$ (calcium carbonate ion activity product/$K_{sp}$) = 4.5; $[Ca]_{TOTAL} = [CO_3^{-2}]_{TOTAL} = 0.0019$ M; $P_{CO2} = 10^{-3.55}$ atm.

[a] CHXHCA = 1,2,3,4,5,6-cyclohexane hexacarboxylic acid (six-carbon ring).

[b] CPRDCA = 1,1-cyclopropane dicarboxylic acid (three-carbon ring).

[c] CBDCA = 1,1-cyclobutane dicarboxylic acid (four-carbon ring).

Calcite growth rates are calculated from the slope of reagent addition (in mL) versus reaction time (in minutes) plots using Equation 2.3. Plots have a zero intercept and good linearity for calcite growth both in the absence and in the presence of PCAs (Figure 2.3 and Tables 2.3 and 2.4). Several alicyclic PCAs reduced calcite crystal growth rates at concentrations of 0.01–0.1 mg/L and stopped calcite crystal growth at solution concentration of 1 mg/L (Tables 2.3 and 2.4). Calcite growth rate inhibition effectiveness of five-atom ring structures with four carboxyl groups can be illustrated by plotting the reduced rate (i.e., $R/R_0$) (Equation 2.4) versus CPETCA

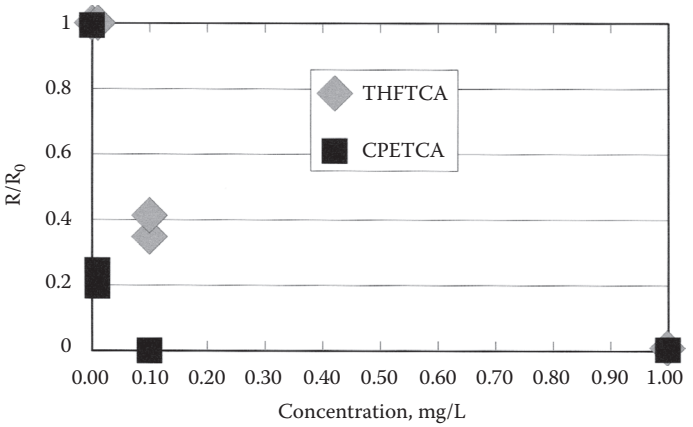


**FIGURE 2.4** Results for experiments with added THFTCA and CPETCA expressed as reduced rates ($R/R_0$). Each point represents one experiment. $R/R_0 = 1$ indicates no crystal growth inhibition.

and THFTCA concentrations (Figure 2.4). Marked calcite growth rate reduction by CPETCA or THFTCA is illustrated in Figure 2.4, where the reduced calcite growth rate exhibits a dramatic decrease with increasing inhibitor concentration (Figure 2.4). CPETCA reduced the calcite growth rate by 80% ($R/R_0 = 0.215 \pm 0.025$ (± 12%) at a solution concentration of 0.01 mg/L. In comparison, CHXHCA is slightly less effective. At a solution concentration of 0.01 mg/L, CHXHCX reduced the calcite growth rate by 65% ($R/R_0 = 0.34 \pm 0.09$ [±30%]) (Table 2.4). In contrast to CHXHCA and CPETCA, THFTCA is a less effective calcite growth rate inhibitor. A 10-fold greater solution concentration of THFTCA is needed to obtain the same calcite growth rate inhibition effectiveness as CHXHCA or CPETCA. THFTCA reduced the calcite growth rate by 65% ($R/R_0 = 0.34 \pm 0.03$ [±9%]) at a solution concentration of 0.1 mg/L (Table 2.3).

There is no induction period for calcite growth in control experiments or in the presence of acyclic or dicarboxylic PCAs. Plots of added titrant versus time are linear for calcite growth rate experiments in the absence of inhibitors and in solutions with low THFTCA concentrations (0.1 mg/L), and there is no induction period (Figure 2.3 and Table 2.3). For higher inhibitor concentrations, the linear fit of mL added versus time plots was less good (R square values were from 0.04 to 0.004; Table 2.3). CHXHCA concentrations of 0.01–0.1 gave a satisfactory fit for mL versus time plots (from 0.96 at 0.01 to 0.27 at 0.1 mg/L; Table 2.4). For concentrations of 0.1 mg/L for CPETCA, and 1 mg/L for CHXHCA and THFTCA, there was little calcite growth.

Unlike control experiments or other inhibitor experiments, growth experiments in solutions with 0.01 mg/L CPETCA (Figure 2.3) exhibit an induction period, followed by a brief (1 min) growth rate surge (at twice the control experiment rate). A time interval of 6.3 ± 0.8 (13%) min (n = 2) was observed before the onset of crystal growth (Figure 2.5). Subsequently, calcite growth occurs at a rate of about twice the control rate for about 1 min followed by a constant rate that is 20% of the control experiment rate (Figure 2.5). Calcite growth in the presence of CPETCA is markedly